IEEE Journal of Microwaves

Received 13 May 2022; revised 13 June 2022; accepted 12 July 2022. Date of publication 29 July 2022; date of current version 7 October 2022.

Digital Object Identifier 10.1109/JMW.2022.3191440

C-Band Septum Polarizers With Polynomial Profile and Accurate Axial Ratio Characterization in Back-to-Back Configuration

NELSON J. G. FONSECA [1] (Senior Member, IEEE), AND JEAN-CHRISTOPHE ANGEVAIN [2]

(Invited Paper)

[1]Antenna and Sub-Millimetre-Waves Section, European Space Agency, 2201 AZ Noordwijk, The Netherlands
[2]Microwave Instruments Section, European Space Agency, 2201 AZ Noordwijk, The Netherlands

CORRESPONDING AUTHOR: Nelson J. G. Fonseca (e-mail: nelson.fonseca@esa.int).

ABSTRACT Septum polarizers have been used in waveguide systems for over 50 years and are very popular in communication satellites operating in circular polarization. With the progress of computational electromagnetics and computer hardware, combined with advances in manufacturing techniques, there has been a growing interest in septum polarizers with smooth profiles. In particular, a design using Legendre polynomials was recently introduced by the authors. This paper reports on the first experimental validation of this component and introduces also alternative profiles based on cubic splines. The new designs account for considerations on the overhang angle, which is an important parameter in additive layer manufacturing. The axial ratio of these designs is evaluated using a simple and accurate technique based on a back-to-back configuration, which can be implemented outside an anechoic chamber. The proposed characterization technique relies on the custom flanges implemented on the circular common port of septum polarizers to interface with horn antennas. These flanges typically have an 8-fold rotational symmetry, which enables to perform multiple measurements of a back-to-back configuration without requiring further equipment. The measured data is then processed to obtain the axial ratio of the two septum polarizers. This characterization technique is particularly advantageous when a large number of feeds needs to be tested, which is relevant in current and future broadband communication satellites. The technique is validated by comparing with measured data acquired in an anechoic chamber using a standard technique. Various prototypes, designed for operation in C-band communication satellite downlink, are characterized and promising results are obtained, showing very good agreement between simulated and measured data.

INDEX TERMS Axial ratio, circular polarization, communication satellite, cross-polarization discrimination (XPD), feed system, guided-mode measurement technique, septum polarizer.

I. INTRODUCTION

Septum polarizers are key elements in microwave systems operating in circular polarization. They are commonly used in waveguide feed systems onboard communication satellites at frequencies ranging from C-band up to Ka-band [1]–[4], avoiding the need for polarization alignment between the onboard and the ground antennas. They are also implemented in ground stations [5], [6] and microwave instruments at millimeter-wave and sub-terahertz frequencies [7]–[9], as well as terrestrial systems, such as surveillance radars and test range probes. The main appeal of this component is to combine high polarization purity over a broad fractional bandwidth of typically 15%–20% and a simple mechanical design compatible with high-precision manufacturing techniques used in space and sub-terahertz systems.

The concept was first introduced in the late 1960's with a simple sloping-septum design [10]. The basic idea is to have a pair of single-mode rectangular waveguides separated

by a thin septum on their common broad wall that transitions along the longitudinal direction into a square waveguide, which supports two degenerate fundamental modes. With a balanced excitation of the modes in phase quadrature, a linearly-polarized signal applied at one of the two rectangular waveguide ports generates a circularly polarized (CP) wave at the common port. Because of the design symmetry, the two rectangular waveguide ports produce orthogonal CP handedness, i.e. one port excites a left hand circularly polarized (LHCP) wave while the other port excites a right hand circularly polarized (RHCP) wave, thus providing the functionality of a CP orthomode transducer (OMT).

Over the years, various design improvements have been proposed. The most widely used design is the stepped septum polarizer [11], which is well suited for standard computer numerical control (CNC) milling. A design with varying thickness was also proposed to increase gradually that parameter away from the common port and provide a more robust mechanical design while maintaining good RF properties [12]. A solution based on a notched septum was proposed in [13], resulting in a very compact implementation at the expense of a narrower fractional bandwidth of about 4%. Several patents were filed in the 1970's up until the 1990's on variations of septum polarizers [14]–[18], confirming the importance of this component in the emerging microwave engineering of the past century. The septum polarizer still inspires new components to this day, including for example the linearly polarized (LP) OMT described in [19], combining an iris polarizer and a septum polarizer, the polarization switch in [20], combining a rotary joint and a septum polarizer, and the directional coupler in [21], which adapts the well-known tandem coupler concept into a tandem polarizer design [22].

With the progress in computational electromagnetics and computer hardware, combined with advances in manufacturing techniques considered for space applications [26], [27], more complex septum profiles have been analysed. For example, Kim *et al.* proposed to replace the conventional stepped profile with a smooth sigmoid profile [23], [24]. This was found to bring benefits in terms of power handling, as removing the sharp edges reduced notably the electric field intensity. However, this comes at the expense of a longer profile for similar functionality, with a reported increase of the septum length in the order of 20% [24]. This is a direct consequence of the formulation employed to define the septum profile which introduces longitudinal tangents at the edges, while a stepped profile is characterized with transversal tangents resulting in a more compact implementation. An alternative smooth profile based on Legendre polynomials was proposed by the authors in [25], observing that odd-degree Legendre polynomials defined along the longitudinal direction provide quasi-transversal tangents at the edge of the septum profile. The specific design in [25] improves the fractional bandwidth by about 15%–20% while reducing the length by 5.5% with reference to a stepped septum polarizer. The profile still avoids sharp edges, which is expected to benefit power handling capabilities. This paper provides the first experimental validation of this concept, with a specific design at C-band. Alternative polynomial profiles are also explored, accounting for additive manufacturing constraints. To facilitate the verification of the different septum profiles, we implemented a mechanical design with removable septum blade and developed a simple back-to-back configuration technique for the accurate characterization of the axial ratio in a laboratory environment.

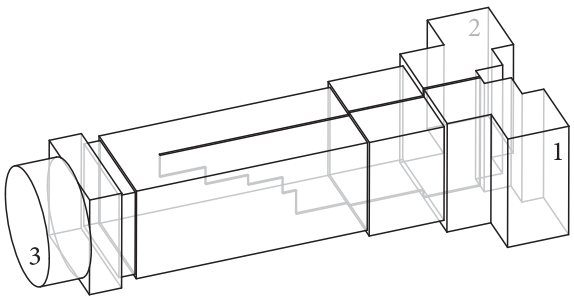

FIGURE 1. Perspective CAD view of a standard stepped septum polarizer and associated port numbering.

The paper is organized as follows. In Section II-A, we first describe the proposed axial ratio characterization technique, relying on the use of standard components only and avoiding the need for a test in an anechoic chamber. The accuracy of this technique is demonstrated in Section II-B, using reference C-band stepped septum polarizers. Section III discusses three designs of septum polarizers shaped with polynomials, supported with numerical results and experimental validation, including the previously reported Legendre polynomial septum polarizer as well as new designs using cubic splines. Finally, Section IV concludes with some perspective on future works.

II. AXIAL RATIO CHARACTERIZATION TECHNIQUE

A. DESCRIPTION

A standard stepped septum polarizer is illustrated in Fig. 1. It has two single-mode rectangular waveguide ports, labeled port 1 and port 2, and a dual-mode circular (or square) waveguide port, labeled port 3. The two degenerate modes at port 3 are orthogonal and may be described in terms of linear components (horizontal and vertical electric field components) or circular components (LHCP and RHCP electric field components). The two field decompositions are related by the formulas

$$\begin{cases} \mathbf{E}_{\mathrm{L}} = \frac{1}{\sqrt{2}} \left(\mathbf{E}_{\mathrm{V}} + j\mathbf{E}_{\mathrm{H}} \right) \\ \mathbf{E}_{\mathrm{R}} = \frac{1}{\sqrt{2}} \left(\mathbf{E}_{\mathrm{V}} - j\mathbf{E}_{\mathrm{H}} \right) \end{cases} \tag{1}$$

where $\mathbf{E}_{\mathrm{V}}$ and $\mathbf{E}_{\mathrm{H}}$ are the vertical and horizontal electric field components, respectively, while $\mathbf{E}_{\mathrm{L}}$ and $\mathbf{E}_{\mathrm{R}}$ are the left hand and right hand CP components, respectively.

The ratio of the co-polarized over the cross-polarized CP components in (1) provides the cross-polarization discrimination (XPD), quantifying the purity of the produced circular polarization. An alternative formulation of this quantity is

the axial ratio (AR), which is a measure of the ellipticity of the polarization produced by the septum polarizer. It is defined as the ratio of the major axis over the minor axis of the ellipse described by the time-varying electric field component in a transversal plane orthogonal to the direction of propagation. Ideally, a circularly polarized electric field has an axial ratio of 1 (0 dB). These two quantities are such that $r = (\rho + 1)/(\rho - 1)$, where r is the AR and ρ the XPD, both being magnitudes expressed with real positive numbers.

The accurate characterization of the AR of a septum polarizer is a problem in itself, as a dual-mode waveguide is not readily characterized without additional test jigs. Septum polarizers are generally connected to horn antennas and thus characterized together in an anechoic chamber. A linearly polarized probe is rotated in front of the antenna under test (AUT) to characterize the AR on-axis. Thanks to the rotational symmetry of a circular horn antenna, its cross-polarization on-axis is very low, thus the measured value on-axis is predominantly set by the septum polarizer. This technique requires accurate alignment between the probe and the AUT as well as low noise interference from the test set-up when low XPD values are to be measured. In general, techniques that need an anechoic chamber lead to a costly and time consuming implementation, even more so at millimeter-wave frequencies. These were still acceptable when a very limited number of feeds had to be characterized. However, current communication satellites use clusters comprising several tens of feeds and future systems are expected to carry up to several hundreds of feeds [28]–[30]. For these reasons, various works report on measurement techniques in guided-mode operation using either specific test jigs (e.g. square-to-rectangular waveguide transitions, dual-linear OMTs) or back-to-back septum polarizers. These techniques can be implemented outside an anechoic chamber and even be automated to some extent, so faulty feeds may be identified prior to integration and more advanced characterization of the complete antenna system in an anechoic chamber. A recent work provided a good overview of characterization techniques for septum polarizers and introduced a simple and accurate approach using different transmission line lengths between two back-to-back septum polarizers [31].

Here, we introduce an even simpler characterization technique focusing on the AR of a septum polarizer. Indeed, the remaining operational parameters, namely the reflection coefficients at port 1 and port 2 as well as the coupling between them, can be characterized by connecting the polarizer to a horn antenna placed in front of an absorbing panel. For these measurements, no positioner nor precise alignment is required, thus the test may be performed outside an anechoic chamber and still provide accurate results. Alternatively, a load may be connected to the common port of the septum polarizer to enable the same characterization without the horn antenna. The typical back-to-back configuration is used differently here. Taking advantage of the fact that septum polarizers designed for feed applications generally have a circular waveguide flange [1]–[4], [6], the relative angular orientation of the two septa, the angle θ illustrated in Fig. 2, may be used as variable in place of multiple line lengths. This flange design enables to perform multiple measurements in back-to-back configuration by simply disconnecting, rotating and reconnecting the two components. This technique may also be implemented inserting a probe with a septum polarizer and a contactless flange design [32], [33] inside a rotationally symmetric horn antenna under test. This approach with a probe is particularly attractive to automatize the testing of large feed arrays.

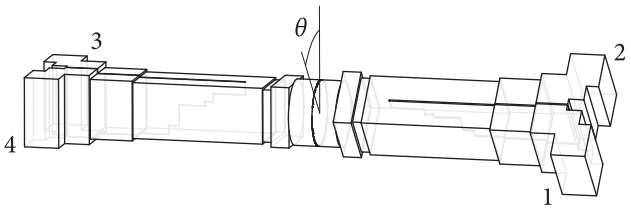

FIGURE 2. Perspective CAD view of the 4-port device formed of back-to-back septum polarizers with associated port numbering and definition of the relative orientation angle θ.

The polarisation loss factor, L_P, may be expressed as a function of θ and of the XPD values of the two back-to-back septa, ρ_1 and ρ_2, as follows [34]

$$L_P = \frac{1 + \rho_1^2\rho_2^2 + 2\rho_1\rho_2\cos 2\theta}{\left(1 + \rho_1^2\right)\left(1 + \rho_2^2\right)}. \tag{2}$$

For given values of ρ_1 and ρ_2, L_P is a periodic function of θ of period π. So the minimum sampling rate, or Nyquist rate, in the angular domain for the function L_P is $2/\pi$, corresponding to samples in θ every 90°. Interestingly, flanges between a horn antenna and a polarizer typically have an 8-fold rotational symmetry, so θ may take 8 different values in discrete steps of 45° from 0° to 315°, which are sufficient to reconstruct numerically the function L_P with no ambiguity. From this, one can extract the numerical values of the maximum and minimum of L_P, $L_P^{\max}$ and $L_P^{\min}$, respectively. From (2), these may be related to ρ_1 and ρ_2 as follows

$$\begin{cases} L_P^{\max} = \frac{(1+\rho_1\rho_2)^2}{(1+\rho_1^2)(1+\rho_2^2)} \\ L_P^{\min} = \frac{(1-\rho_1\rho_2)^2}{(1+\rho_1^2)(1+\rho_2^2)} \end{cases} \tag{3}$$

It is apparent from (2) and (3) that these expressions are symmetric with respect to ρ_1 and ρ_2, which may not be differentiated without further information. In practice, this means that either a known septum polarizer, which may have been characterized using an alternative technique, has to be used as reference to evaluate the XPD of the septum polarizer under test or that at least three septum polarizers need to be tested back-to-back with the proposed technique. Accounting for the symmetry of the problem, we introduce Π and Σ as the product and sum of ρ_1 and ρ_2, respectively, i.e. $\Pi = \rho_1\rho_2$ and $\Sigma = \rho_1 + \rho_2$. Using (3), the ratio $L_P^{\max}/L_P^{\min}$ leads, after some

algebra, to the following

$$\Pi = \frac{\sqrt{L_P^{\max}} - \sqrt{L_P^{\min}}}{\sqrt{L_P^{\max}} + \sqrt{L_P^{\min}}}. \tag{4}$$

Knowing Π, one can evaluate the remaining unknown Σ using one of the two equations in (3). For example, using the expression for $L_P^{\max}$, the following equation is obtained after some manipulations and simplifications

$$\Sigma = \sqrt{\frac{(1+\Pi)^2}{L_P^{\max}} - (1-\Pi)^2}. \tag{5}$$

The XPD values of the two septum polarizers under test are thus given as

$$\begin{cases} \rho_1 = \frac{\Sigma}{2} - \sqrt{\left(\frac{\Sigma}{2}\right)^2 - \Pi} \\ \rho_2 = \frac{\Sigma}{2} + \sqrt{\left(\frac{\Sigma}{2}\right)^2 - \Pi} \end{cases} \tag{6}$$

The assignment with the plus and minus signs is obviously arbitrary as explained above, due to the symmetry of the problem. The AR values r_1 and r_2 are then determined.

The starting point of the proposed AR characterization technique is the measurement of the polarization loss factor, L_P. The 4-port device obtained with back-to-back septum polarizers, as illustrated in Fig. 2, operates ideally as a cross-over. Neglecting all losses and assuming the two septum polarizers produce perfect circular polarization, a signal applied at port 1 is fully directed to port 3, while a signal applied at port 2 is directed to port 4. Accounting for reflection and isolation losses, the polarisation loss factor, with reference to port 1, may be defined as

$$L_P = \frac{|S_{13}|^2}{|S_{13}|^2 + |S_{14}|^2}, \tag{7}$$

where S_{ij} are scattering parameters of the 4-port device formed by the back-to-back polarizers with the port numbering defined in Fig. 2. The polarization loss factor is thus defined as the ratio of the transmitted co-polarized field power over the total transmitted power. These parameters are measured as a function of frequency over the range of interest for each value of θ.

The proposed AR characterization technique is thus defined as follows:

a) Measure the complete S-matrix of the back-to-back septum polarizer 4-port device as a function of frequency for each angular position θ;
b) Use (7) to evaluate the polarization loss factor, L_P, as a function of frequency for each angular position θ;
c) Use an adequate interpolation method to evaluate numerically L_P as a function of θ for each frequency point, with sufficient sampling to accurately determine its maximum and minimum values, $L_P^{\max}$ and $L_P^{\min}$, as functions of frequency;
d) Use (4)–(6) to determine successively the product Π of the XPD values of the two septum polarizers, ρ_1 and ρ_2, as a function of frequency, the sum Σ of ρ_1 and ρ_2, as a function of frequency, and finally ρ_1 and ρ_2 from Π and Σ as functions of frequency;
e) Obtain the AR values of the two septum polarizers, r_1 and r_2, as functions of frequency using the expression $r = (\rho + 1)/(\rho - 1)$.

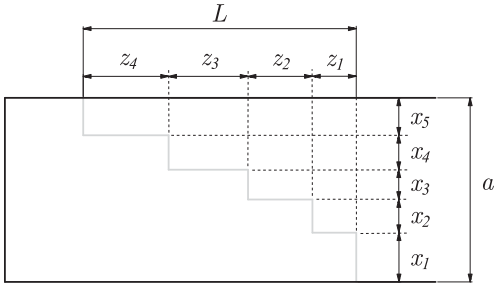

FIGURE 3. Design parameters of a standard stepped septum polarizer of length *L* in a square waveguide of side *a*.

Applying this simple procedure once, two AR values are obtained for each frequency point. Note that with the notations in (6), $\rho_1 \leq \rho_2$ for any frequency point, and thus $r_1 \geq r_2$. The ambiguity between the two curves as functions of frequency occur when they cross. If one of the two septum polarizers has already been characterized and its AR is known, this information may be used to identify the AR of the septum polarizer under test. Preferably, the reference polarizer shall have a response distinct from the one of the polarizer under test to facilitate the differentiation, accounting for measurement uncertainties. In case no reference polarizer is available, the procedure shall be applied twice using 3 septum polarizers. Testing first polarizers 1 and 2 back-to-back, then polarizers 1 and 3 back-to-back, one can identify the AR of the septum polarizer 1 comparing the numerical results of the two tests, taking also into consideration measurement uncertainties, and then deduce the AR of the polarizers 2 and 3 as being the remaining curves in the respective test results.

B. VALIDATION

In this section, we provide an experimental validation of the proposed AR characterization technique based on a back-to-back configuration by comparing with a standard characterization technique in anechoic chamber. To this end, two C-band stepped septum polarizers are designed with different specifications to distinguish their response using our technique. The design parameters of the septum profile are defined in Fig. 3. The overall waveguide component design is the same for all septum polarizers discussed in this paper, so only two identical split-block components are manufactured and the septum blades may be interchanged to characterize multiple polarizer designs. All the blades are designed with a length $L = 65$ mm and a thickness $t = 1$ mm. The square waveguide in which the septum blade is clamped has a side $a = 47$ mm. These parameter values were found to be acceptable for all profile designs.

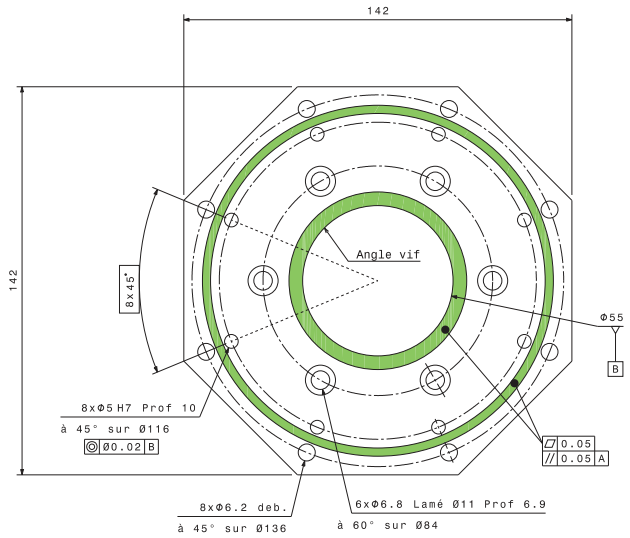

FIGURE 4. Mechanical drawing of the flange at the common circular waveguide port with an 8-fold rotational symmetry enabling multiple angular orientations between the back-to-back septum polarizers.

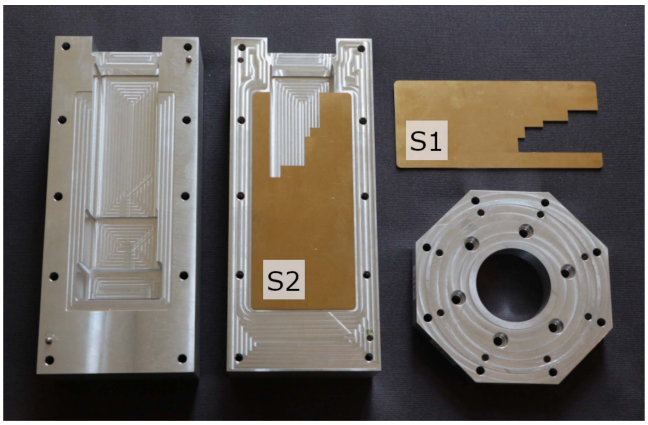

FIGURE 5. Mechanical parts of the designed C-band septum polarizer (made of aluminum) and stepped septum blades (made of brass).

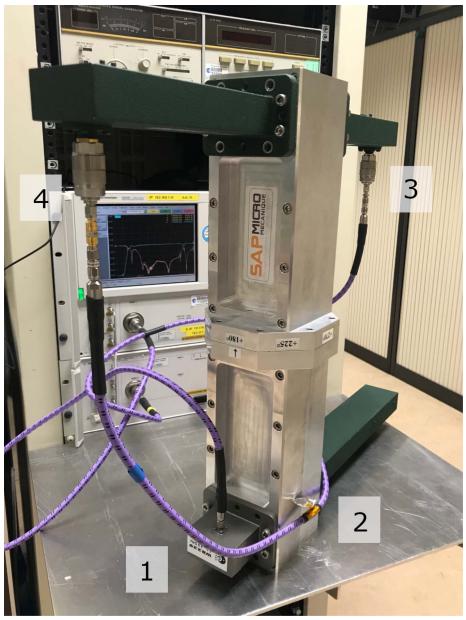

FIGURE 6. Test set-up of the proposed axial ratio characterization technique using a back-to-back septum polarizer configuration in the ESA Microwave Laboratory and associated port numbering.

The first stepped septum polarizer, labeled S1, is set to provide low AR over a reduced bandwidth (3.7–4.1 GHz) with a design specification set to 0.15 dB. This corresponds to an XPD better than 40 dB. The reflection coefficients at port 1 and port 2 and coupling between these two ports are specified to be lower than −25 dB over the operating frequency range. The model is optimized using the EM solver HFSS. The obtained parameters are $x_1 = 12.57$ mm, $x_2 = 8.48$ mm, $x_3 = 5.12$ mm, $x_4 = 9.09$ mm, $z_1 = 6.47$ mm, $z_2 = 16.43$ mm and $z_3 = 20.29$ mm. With the design constraint on a and L, the remaining parameters are $x_5 = 11.74$ mm and $z_4 = 21.81$ mm. A second stepped septum polarizer, labeled S2, is set to operate over a wider bandwidth (3.6–4.2 GHz) corresponding to the nominal C-band allocated to satellite downlink, with a design specification of 0.3 dB (XPD better than 35 dB). The reflection and coupling coefficients of the ports 1 and 2 are also set to −25 dB over the specified frequency band. The optimized parameters are $x_1 = 7.58$ mm, $x_2 = 17.59$ mm, $x_3 = 3.61$ mm, $x_4 = 7.07$ mm, $z_1 = 8.74$ mm, $z_2 = 22.00$ mm and $z_3 = 6.93$ mm. The remaining parameters are $x_5 = 11.15$ mm and $z_4 = 27.33$ mm. These specifications are quite demanding as broadcasting applications typically require very low cross-polarization. This is an interesting test case for our characterization technique as very low AR values are obviously more difficult to measure accurately.

To complete the design of the prototypes, transitions and bends, visible in the CAD views of Figs. 1 and 2, are added to facilitate the integration of standard WR229 flanges for test purposes. They are designed with minimal impact on the overall RF properties. A custom interface is used on the common circular port with an 8-fold rotational symmetry, as detailed in the mechanical drawing reported in Fig. 4. A picture of the mechanical parts of one of the two identical split-block prototypes is provided in Fig. 5, also including the septum blades S1 and S2. These parts were manufactured by SAP Micro-mécanique, Ambres, France, using high precision CNC milling. The waveguide parts are made of aluminum, while the blades are made of brass, which is easier to machine and thus well suited for the more advanced polynomial profiles. The electrical conductivity of brass ($\sigma \approx 1.6 \times 10^7 \mathrm{S.m}^{-1}$) is about half that of aluminum, which was found to have very marginal impact on performance. The test set-up in the ESA Microwave Laboratory with back-to-back septum polarizers corresponding to the proposed AR characterization technique is shown in Fig. 6. Using a Vector Network Analyzer (VNA) with 4 ports, one can acquire the complete matrix for each θ position. In the test set-up of Fig. 6, the isolated port (port 2) is effectively loaded to reduce the amount of data to be processed, as the response of the structure is symmetric with

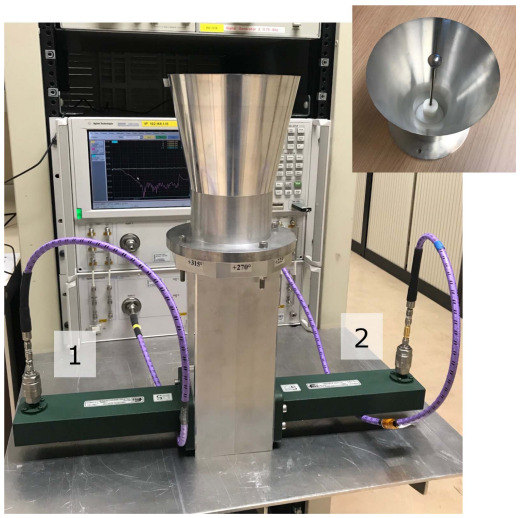

FIGURE 7. Test set-up for the characterization of a septum polarizer using a custom horn design and associated port numbering (inset: test jig with sphere target inserted in the horn for alignment in CATR).

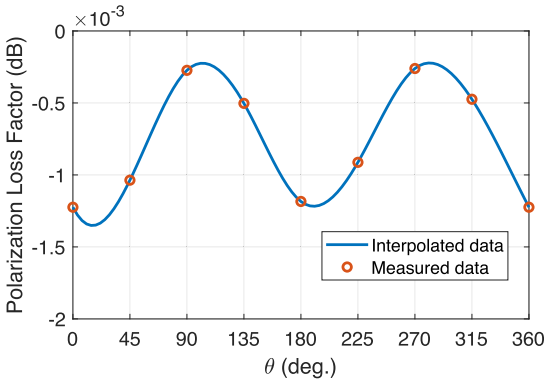

FIGURE 8. Interpolation of the polarization loss factor as a function of the angular orientation, θ, between the back-to-back septum polarizers S1 and S2, from measured data at 3.9 GHz.

reference to port 1 and port 2. In Fig. 7, one of the septum polarizers is shown connected to the custom horn designed for testing in the ESA Compact Antenna Test Range (CATR). The horn was designed to provide a return loss better than 30 dB over the band of interest. The inset in Fig. 7 shows the test jig with the sphere target to be inserted in the horn during the alignment procedure. This tool enables alignment using a laser tracker, which is more accurate than RF alignment (e.g. based on maximum gain).

Following the proposed procedure, the polarization loss factor, L_P, is evaluated as a function of θ for each frequency point using a cubic interpolation in MATLAB with sufficient sampling to have an accurate evaluation of $L_P^{\max}$ and $L_P^{\min}$. An example of this interpolation process is provided in Fig. 8 with data measured at 3.9 GHz, corresponding to the center frequency of the operating bands. Although the polarization loss measured is very low, owing to the excellent AR of the two stepped septum polarizers over the operating band, the measured data is fairly periodic as expected from theory. The

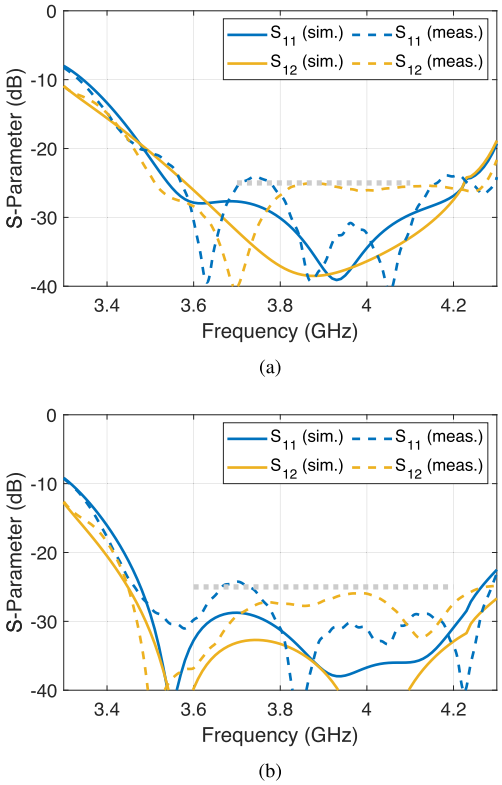

FIGURE 9. Simulated and measured S-parameters of the stepped septum polarizers (a) S1 and (b) S2 (design specifications in gray dashed lines).

main discrepancy with the reported data appears on the minimum value, with an error in the order of 10% of the dynamic range under characterization, $L_P^{\max} - L_P^{\min}$, corresponding to an uncertainty of a few hundredths of dB on the AR. This is considered excellent in view of the simplicity of the proposed technique.

Numerical results are reported in Fig. 9 for selected S-parameters, specifically the reflection coefficient at port 1 (port 2 is symmetric) and the coupling coefficient between port 1 and port 2. The simulation results obtained with HFSS for the septum polarizers as stand-alone component (i.e. not connected to the horn antenna nor in back-to-back configuration) are compared to the corresponding measured results in the ESA Microwave Laboratory with the horn placed in front of an absorbing panel for S1 and S2 in Fig. 9(a) and Fig. 9(b), respectively. While there are some visible discrepancies between simulation and measurement, which can be attributed to manufacturing and assembling uncertainties as well as measurement errors, the parameters remain below -24 dB. The results are sufficient to ensure that these losses do not affect notably the evaluation of the AR, reported in Fig. 10. Specifically, Fig. 10(a) presents the simulation results obtained with HFSS for the septum polarizers as stand-alone component for reference. These results show the excellent performance obtained over the respective bandwidths with the two stepped septum designs. In Fig. 10(b), the numerical results obtained using the measured data and the proposed characterization technique are reported in raw format, i.e. the two AR curves

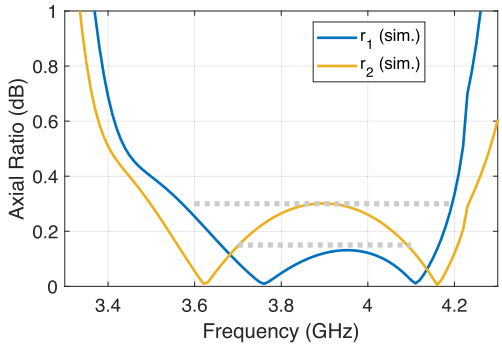

(a)

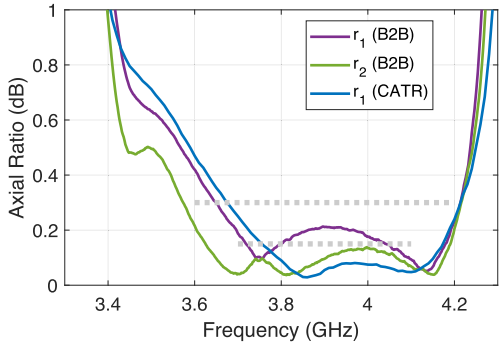

(b)

FIGURE 10. Axial ratio of the two stepped septum polarizers, S1 and S2: (a) simulation results and (b) measurement results (design specifications in gray dashed lines).

are not differentiated at this stage. With the notations in (6), ρ_1 corresponds to the lower XPD value, thus r_1 is associated to the larger of the two AR values (purple curve), while r_2 is the smaller one (green curve). As expected by design, the two curves are mostly distinct over the considered bandwidth. A slight frequency shift is observed which makes the two curves more difficult to differentiate in the upper range of the measured frequency band (4.1–4.3 GHz). The septum polarizer S1 was also measured in the CATR and the numerical results are overlaid in Fig. 10(b) (blue curve). These results also display a slight frequency shift, which confirms this discrepancy is due to residual manufacturing and assembling errors rather than measurement errors. The manufacturing and assembling tolerances were evaluated in the order of $\pm 30\mu$m, which is generally acceptable for waveguide parts in C-band. With the split-block approach implemented here, manufacturing errors can affect the balance between the two fundamental modes in the square waveguide section containing the septum blade. An error of $\pm 30\mu$m leading to a slightly rectangular waveguide can generate an error in phase in the order of 1°, equivalent to a variation in the AR in the order of 0.15 dB, in line with observed deviations. Despite these discrepancies, the curve measured in the CATR follows reasonably well the results obtained with our proposed technique, enabling to identify the numerical results corresponding to S1 over most of the analyzed frequency band (3.3–4.1 GHz). Above 4.1 GHz, the results are all very similar and more difficult to distinguish. The difference between the two measurement techniques is below 0.05 dB over the range 3.55–4.25 GHz, covering the frequency band of interest. This frequency range corresponds to the bandwidth over which the reflection and coupling coefficients of the septum polarizers are low, especially the reflections at the common port. This is particularly important to ensure a stable response when connecting two septum polarizers back-to-back. These results validate the accuracy of the proposed technique, which is used to characterize new septum polarizer designs in Section III.

III. SEPTUM POLARIZERS WITH POLYNOMINAL PROFILE

Over recent years, there has been a growing interest in septum polarizers with smooth profiles. Besides the sigmoid design discussed in the introduction [23], [24], a Ku-band prototype manufactured using direct metal laser sintering has been reported in [35]. This design uses piecewise cubic Hermite interpolating polynomials (PCHIP), as an alternative to Legendre polynomials [25]. This section discusses the first experimental validation of a septum polarizer with a profile based on Legendre polynomials as well as other polynomial profiles more adapted to additive manufacturing [36].

A. LEGENDRE POLYNOMINALS

As discussed in [25], odd-degree Legendre polynomials have a shape well suited for the design of septum polarizers. This solution is adapted here to C-band applications and the septum blade is labeled L1. The length of the septum is kept equal to 65 mm for direct comparison with the designs discussed in Section II. All other component parameters are also kept unchanged, including the size of the waveguide in which the septum blade is clamped ($a = 47$ mm). The specification on the AR is further relaxed in an attempt to increase the frequency bandwidth. The design prototyped has an AR better than 0.4 dB over the frequency band 3.5–4.2 GHz, corresponding to a fractional bandwidth of 18.2%. Similarly to the design in [25], the first 9 Legendre polynomials are considered and the profile is optimized using a full-wave model implemented in HFSS. The weighting coefficients are $a_1 = 1.357$, $a_2 = -0.226$, $a_3 = 0.181$, $a_4 = -0.523$, $a_5 = -0.221$, $a_6 = 0.106$, $a_7 = 0.427$, $a_8 = 0.05$ and $a_9 = 1$. The coefficients are normalized to a_9, corresponding to the coefficient of the Legendre polynomial of order 9, as the profile is further normalized to adjust the height of the septum to fit the dimension of the waveguide cross-section a, leading to 8 independent optimization variables. The corresponding profile is illustrated in Fig. 11(a) and the manufactured blade is shown in Fig. 12 together with the other blades. The numerical results obtained with the full-wave model are reported in Fig. 13(a), where they are compared to the AR of the other designs. The measured reflection and coupling coefficients are better than -23 dB (-25 dB in simulation) over the design frequency band and are not reported here, as they are very similar to those provided in Section II. The septum polarizer is tested in back-to-back configuration using the septum polarizer S1 as reference. The measured AR is reported in Fig. 13(b), where

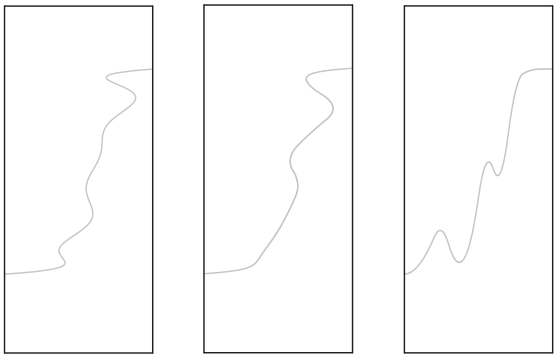

FIGURE 11. Septum polarizers with polynomial profile: (a) Legendre polynomials, (b) probit-like function modulated using cubic splines and (c) transversal piecewise cubic splines.

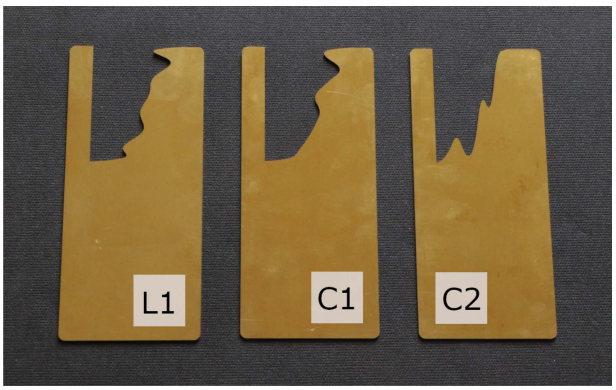

FIGURE 12. Manufactured septum blades shaped with Legendre polynomials (L1), with a probit-like function modulated using cubic splines (C1) and with transversal piecewise cubic splines (C2).

it is compared to the measured AR of the other designs to facilitate a direct comparison between the different polynomial profiles as only the blades are changed between different test result acquisitions. A reasonably good agreement is found between simulated and measured data, in line with the results reported in Section II with a similar frequency shift attributed to manufacturing and assembling tolerances. The response shows a slight reduction in operating bandwidth, together with a small reduction of the AR value around the center frequency. An AR better than 0.4 dB is obtained in measurement over the frequency band 3.54–4.18 GHz, corresponding to a fractional bandwidth of 16.6% (18.7% in simulation). The worst case measured AR over the design frequency is 0.53 dB (0.36 dB in simulation). The importance of a symmetric cross-section to achieve high polarization purity is the main reason feed systems are generally printed along their longitudinal direction. This adds constraints to the profile design addressed in the following section.

B. PROBIT-LIKE FUNCTION WITH CUBIC SPLINES

As discussed in [36], the shape of the septum polarizer using Legendre polynomials is not well suited for additive manufacturing. Some parts having stronger variations (e.g. top edge of the profile in Fig. 11(a)) would result in large overhang

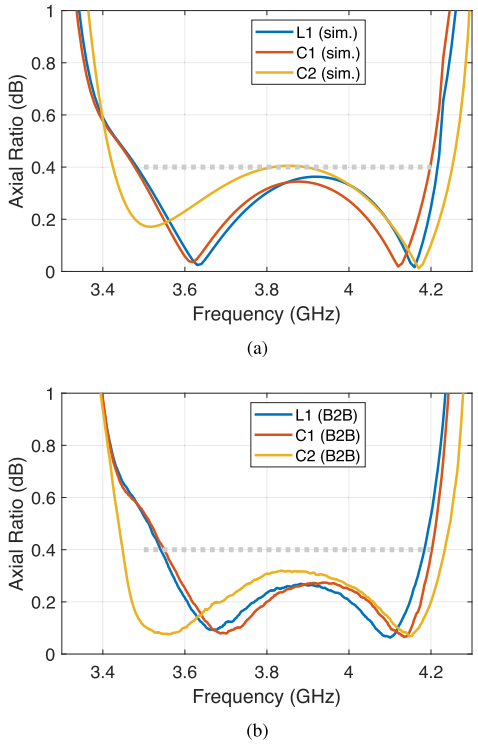

FIGURE 13. Axial ratio of the septum polarizers shaped with polynomials: (a) simulation and (b) measurement results (design specifications in gray dashed lines).

angle values when printing along the longitudinal direction (vertical direction in Fig. 11 and Fig. 12). These variations are introduced by the higher order Legendre polynomials, which are also necessary to ensure a quasi-transversal tangent on the edges of the profiles. For these reasons, it is difficult to find a design based on Legendre polynomials that combines optimal RF properties and mechanical constraints. In addition, the optimization of such profiles converges rather slowly. As the polynomials are defined over the complete length of the profile, a change in weighting coefficient affects the complete profile, which may result in antagonistic effects on RF properties. A piecewise approach, like the one implemented in the stepped septum design or the PCHIP profile in [35], would provide more flexibility to adjust locally the shape of the septum profile.

As mentioned in the introduction, the sigmoid function is not an optimal choice as it extends in the longitudinal direction and affects the length of the septum polarizer. In fact, the inverse of a sigmoid would be better adapted to define the shape of the septum polarizer, such as the probit function, which is the inverse of the cumulative distribution function of the standard normal distribution. However, this function is not straightforward to implement in a full-wave model. We use instead an approximation based on odd-order polynomials defined with the following parametric function

$$\begin{cases} x(t) = a\left(\frac{h(2t-1)^p+2t-1}{2h+2} + \frac{1}{2}\right) \\ z(t) = Lt \end{cases} \tag{8}$$

TABLE 1. Comparison With Existing Septum Polarizer Designs

Reference	Manufacturing Technique	Profile Type	Common Waveguide Cross-section	Frequency Band	Fractional Bandwidth	Return Loss	Isolation	Axial Ratio
[1]	CNC Milling	Stepped	Square	C-band (5.85–6.17 GHz)	5.3%	37 dB*	32 dB*	0.1 dB*
[6]	CNC Milling	Stepped	Circular	X-band (7.7–8.5 GHz)	9.9%	18 dB	20 dB	–
[7]	CNC Milling	Stepped	Square	EHF (213–237 GHz)	10.7%	20 dB	30 dB	1.4 dB
[12]	–	Stepped-thickness	Square	K-band (16.0–18.9 GHz)	16.6%	22 dB*	22 dB*	0.5 dB*
[23]	–	Smooth Sigmoid	Circular	C-band (5.075–6.525 GHz)	25%	15 dB*	17 dB*	2 dB*
[38]	3D Printing	Stepped	Triangular	K-band (17.9–26.2 GHz)	37.6%	14 dB	17 dB	1.3 dB
This work (III.A)	CNC Milling	Legendre polynomials	Square	C-band (3.54–4.18 GHz)	16.6%	22.4 dB	25.2 dB	0.4 dB
This work (III.B)	CNC Milling	Longitudinal cubic spline	Square	C-band (3.55–4.20 GHz)	16.8%	21.9 dB	22.5 dB	0.4 dB
This work (III.C)	CNC Milling	Transversal cubic spline	Square	C-band (3.5–4.2 GHz)	18.2%	21.3 dB	23.5 dB	0.32 dB

*Simulated value. All other values reported in this Table are based on measured data.

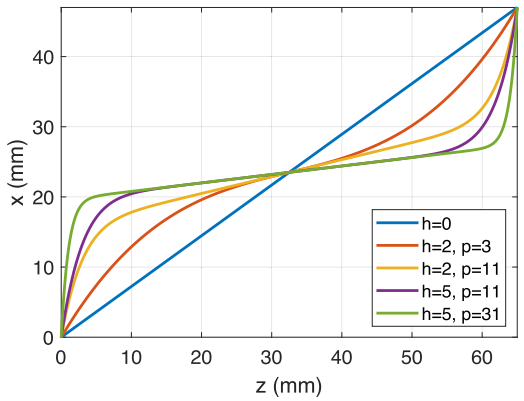

FIGURE 14. Probit-type function for the definition of the general shape of a septum polarizer modulated with longitudinal cubic splines.

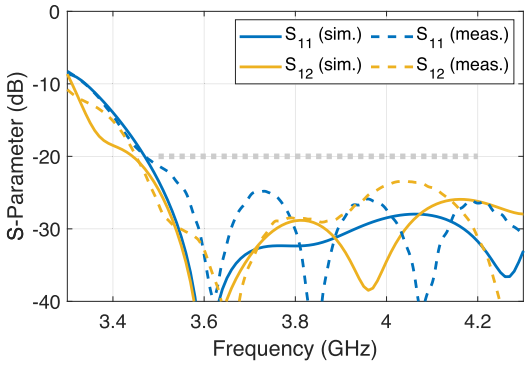

FIGURE 15. Simulated and measured S-parameters of the septum polarizers C2 shaped with transversal cubic splines (design specifications in gray dashed lines).

where x and z are functions of $t \in [0, 1]$ describing the septum profile along the transversal and longitudinal directions, respectively, while p and h are an odd integer and a positive real number, respectively, used to adjust the shape of the profile. Numerical values for different sets of parameters are reported in Fig. 14, which highlight how the parameter p may be used to adjust the tangents at the edges of the profile, while the parameter h mostly defines the tangent at the center. The particular case $h = 0$ corresponds to the original sloping septum described in [10]. Rather than cascading several of these functions as done in [23], [24] with sigmoid functions, we use instead this function to define the general shape of the septum and modulate it using cubic splines, which proved effective to modulate the profile of geodesic lenses in [37]. This piecewise spline formulation along the longitudinal direction enables to adjust locally the shape of the septum, which speeds up the convergence and also facilitates the control of the shape to reduce overhanging parts. The cubic spline formulation used is equal to zero and has longitudinal tangents at the edges of the profile, so this part of the curve is predominantly controlled by the base function in (8). The optimized profile is reported in Fig. 11(b) and the corresponding septum blade is labeled C1. The piecewise function is set to have regular intervals of size $t_{i+1} - t_i = 0.125$, leading to 6 weighting coefficients for optimization, which together with the 2 parameters of the base function in (8) provides the same number of optimization variables as in the Legendre polynomial solution. The numerical values obtained are $h = 2$, $p = 31$, $P_0 = 0.089$, $P_1 = 0.141$, $P_2 = 0.174$, $P_3 = 0.027$, $P_4 = 0.155$ and $P_5 = 0.325$. The coefficients P_i are normalized and the cubic spline function is further multiplied by a and added to the base function in (8) to produce the final septum profile. The AR obtained with the full-wave model is reported in Fig. 13(a), while the measured results, using the back-to-back configuration, are provided in Fig. 13(b). The reflection and coupling coefficients are by design better than -25 dB and below -22 dB

in measurements, in line with the results discussed in Section II. The RF properties are found to be very similar to those obtained with Legendre polynomials although the profile is smoother. The measured AR is below 0.4 dB over the frequency band 3.55–4.20 GHz, corresponding to a fractional bandwidth of 16.8% (18.8% in simulation), comparable to the performance of the Legendre polynomial design. The worst case measured AR over the design frequency is 0.54 dB (0.42 dB in simulation). With this design, the overhang angle remains below 45° when printing along the longitudinal direction, although it gets close to the limit on the top end of the profile as shown in Fig. 11(b), which triggered the solution discussed next.

C. TRANSVERSAL CUBIC SPLINES

To resolve the problem of the overhang angle while minimizing the impact on RF properties, we explore here a different approach further inspired from the modulated geodesic lens design in [37]. The length of the septum polarizer L is generally larger than the cross-section size a. For this reason it is quite intuitive to modulate the profile along the longitudinal direction as this provides more space for advanced shapes. The design proposed here demonstrates that modulation along the transversal direction is also a working solution. Using the cubic spline function of the previous section along the transversal direction, the resulting profile has transversal tangents at the edges, which is favorable. However, a definition of the function along the cross-section of the waveguide would result in the two edges having the same longitudinal position, similarly to the notched septum design in [13]. This could be of interest for compact designs but would drastically reduce the operating bandwidth. Here, we use instead a symmetric spline function as defined in [37] across the diameter of the lens, i.e. the waveguide cross-section corresponds to a "radius" or half of the abscissa range of the spline function. The optimized profile is shown in Fig. 11(c) and the corresponding septum blade is labeled C2 in Fig. 12. The piecewise function is set to have regular intervals of size $t_{i+1} - t_i = 0.05$, corresponding to 10 normalized segments across the waveguide dimension a and 8 independent optimization variables, for a fair comparison with previous designs. The numerical values are $P_0 = 0.0928$, $P_1 = 0.2628$, $P_2 = 0.0201$, $P_3 = 0.1236$, $P_4 = 0.6250$, $P_5 = 0.3996$, $P_6 = 0.9564$ and $P_7 = 0.9975$. These values are normalized to the septum length $L = 65$ mm. The value $P_8 = 1.0012$ is constrained such that the spline function returns the value L for $t = 0.5$ and $P_9 = P_7$ for symmetry, which ensures a transversal tangent at $t = 0.5$. The simulated AR is reported in Fig. 13(a), while the measured results are shown in Fig. 13(b). This design is shown to perform quite well in comparison with the other designs. It has a slightly higher AR within the operating bandwidth, yet within the specification of 0.4 dB. The frequency bandwidth with a measured AR below 0.4 dB is 3.45–4.23 GHz, corresponding to a fractional bandwidth of 20.3% (21.4% in simulation). The worst case measured AR over the design frequency is 0.32 dB (0.4 dB in simulation). The differences between simulated and measured data are well within the deviations discussed previously in connection with manufacturing and assembling errors. The simulated reflection and coupling coefficients are similar to the other designs, with values below −25 dB across the operating frequency. The corresponding measured results are better than −21 dB over the nominal bandwidth and better than −18 dB over the extended bandwidth with an AR below 0.4 dB. These are reported in Fig. 15, to demonstrate the good performance of this design, which differs from the other polynomial designs already reported, particularly in the bottom edge of the profile as visible in Figs. 11 and 12. These results confirm that septum profiles modulated along the transversal direction may perform just as well as more conventional designs. This design shows very promising RF properties combined with a profile more adapted to additive layer manufacturing. As this specific design was constrained by the waveguide size and septum length, which had to be identical for all designs, it is anticipated that further improvement in performance may still be possible adjusting all parameters with this type of polynomial function.

A similar profile characteristic with no overhang angle would be possible enforcing the polynomial function defined along the longitudinal direction to be monotonic. This is the case of the sigmoid profiles proposed in [23], [24]. However, in these particular cases the monotonic function implemented resulted in a longer septum profile. This topic is certainly worth exploring further as other monotonic functions may prove to be more advantageous. Variants of stepped profiles without sharp edges (e.g. chamfered or rounded corners) may also be considered to improve power handling. Recent works have explored less conventional common waveguide cross-sections, such as the triangular waveguide design with a 38% fractional bandwidth reported in [38], as well as operation beyond the fundamental mode bandwidth for dual-band feed systems in [39]. Interesting designs may be obtained combining these concepts with the proposed cubic spline profiles. The results reported in this paper are summarized in Table 1, where they are also compared to alternative solutions in terms of geometrical and RF properties. The designs described in this work indicate that with adequate optimisation, the RF properties of septum polarizers are primarily driven by the waveguide cross section and length of the septum, while the profile may be used for second order adjustment of the performance, particularly on the fractional bandwidth. This provides some freedom to better adjust the septum profile to the constraints of a given manufacturing technique.

IV. CONCLUSION

This paper provided a detailed discussion of septum polarizers with polynomial profiles. These smooth designs have gained some attention over recent years as they have demonstrated benefits in terms of power handling and are well suited for alternative manufacturing techniques, such as additive layer

manufacturing. The axial ratio, characterizing the polarization purity of the device, is a key parameter that generally requires advanced testing techniques to achieve accurate measurement. We proposed here a simple and accurate technique in guided-mode based on a back-to-back arrangement of two septum polarizers, which may have different designs and performance. In fact, having different designs facilitates the differentiation, as demonstrated in this paper. This technique is particularly attractive for the characterization of large feed array systems used in broadband communication satellites. The characterization technique has been validated by comparison with data acquired in an anechoic chamber. The maximum deviation over the frequency band of interest is found to be less than 0.05 dB in C-band, well in line with typical measurement uncertainties. This characterization technique was then used to test three different septum polarizer designs with polynomial profiles, including one using Legendre polynomials. Alternative profiles using cubic splines were characterized and demonstrated excellent RF properties, while reducing the overhang angle assuming additive layer printing along the longitudinal direction of the feed. The designs were all optimized to operate over the portion of the C-band allocated to communication satellite downlink. Excellent agreement was found between simulated and measured data.

The proposed technique is of interest for automated characterization of advanced feed clusters having a large number of feeds. Future investigations will assess the accuracy of this technique applied to millimeter-wave feed systems. Another interesting path for future work includes the design and manufacture of septum polarizers at Ku and Ka-band using the proposed transversal cubic splines combined with additive layer manufacturing techniques.

ACKNOWLEDGMENT

The authors thank Eric van der Houwen and Ines Barbary, from ESA, Noordwijk, The Netherlands, for the support related to the tests in the CATR, as well as Gearoid Loughnane and Cesar Miquel Espana, also from ESA, for the support related to the tests in the Microwave Laboratory. The authors also want to acknowledge Cedric Batut and Patrick Delazzari, from SAP Micro-mécanique, Ambres, France, for the support on the mechanical design and manufacturing of the prototypes, as well as Andre Zandvliet and Stefano Trombini, from the ESA mechanical Workshop.

REFERENCES

[1] R. Garcia, F. Mayol, J. M. Montero, and A. Culebras, "Circular polarization feed with dual-frequency OMT-based turnstile junction," *IEEE Antennas Propag. Mag.*, vol. 53, no. 1, pp. 226–236, Feb. 2011.

[2] R. Ravanelli et al., "C band self diplexed tx/rx feed system for telecom," in *Proc. 14th Eur. Conf. Antennas Propag.*, Copenhagen, Denmark, 2020, pp. 1–4.

[3] P. Lepeltier, P. Bosshard, J. Maurel, C. Labourdette, G. Navarre, and J. David, "Recent achievements and future trends for multiple beam telecommunication antennas," in *Proc. IEEE Int. Symp. Antenna Tech. Appl. Electromagn.*, Toulouse, France, 2012, pp. 1–6.

[4] U. Hong, M. Schneider, and R. Gehring, "Slim Ka-band triple band polariser network for user and gateway antenna feed application," in *Proc. 47th Eur. Microw. Conf.*, Nuremberg, Germany, 2017, pp. 1163–1166.

[5] A. Giacomini, L. J. Foged, R. Morbidini, A. Potenza, J. P. Abadie, and J. Mongis, "S-band feeder for balloon ground station system," in *Proc. IEEE Int. Symp. Antennas Propag.*, Chicago, USA, 2012, pp. 1–2.

[6] S. S. Roy et al., "Design of a compact multielement monopulse feed for ground-station satellite tracking applications," *IEEE Antennas Wireless Propag. Lett.*, vol. 18, no. 9, pp. 1721–1725, Sep. 2019.

[7] C. A. Leal-Sevillano, K. B. Cooper, J. A. Ruiz-Cruz, J. R. Montejo-Garai, and J. M. Rebollar, "A 225 GHz circular polarization waveguide duplexer based on a septum orthomode transducer polarizer," *IEEE Trans. THz Sci. Technol.*, vol. 3, no. 5, pp. 574–583, Sep. 2013.

[8] Y.-L. Chen, T. Chiueh, and H.-F. Teng, "A 77-118 GHz resonance free septum polarizer," *Astrophys. J. Suppl.*, vol. 211, no. 1, pp. 1–11, Mar. 2014.

[9] Y. Hasegawa et al., "A new approach to suppress the effect of machining error for waveguide septum circular polarizer at 230 GHz band in radio astronomy," *J. Infrared, Millimeter, THz Waves*, vol. 38, no. 5, pp. 638–652, Feb. 2017.

[10] D. Davis, O. J. Digiondomenico, and J. Kempic, "A new type of circularly polarized antenna element," in *Proc. IEEE Antennas Propag. Soc. Int. Symp.*, 1967, pp. 26–33.

[11] M. H. Chen and G. N. Tsandoulas, "A wide-band square-waveguide array polarizer," *IEEE Trans. Antennas Propag.*, vol. AP-21, no. 3, pp. 389–391, May 1973.

[12] J. Bornemann and V. A. Labay, "Ridge waveguide polarizer with finite and stepped-thickness septum," *IEEE Trans. Microw. Theory Techn.*, vol. 43, no. 8, pp. 1782–1787, Aug. 1995.

[13] N. C. Albertsen and P. Skov-Madsen, "A compact septum polarizer," *IEEE Trans. Microw. Theory Techn.*, vol. 31, no. 8, pp. 654–660, Aug. 1983.

[14] E. Salzberg, "Microwave hybrid polarizer," U.S. Patent 4,122,406, Oct. 1978.

[15] H. J. Gould, "Balanced phased septum polarizer," U.S. Patent 4,126,835, Nov. 1978.

[16] A. B. C. Davies and A. P. Norris, "Waveguide junction for producing circularly polarized signal," U.S. Patent 4,395,685, Jul. 1983.

[17] M. N. Wong, "Horn radiator assembly with stepped septum polarizer," Eur. Patent 0577320, Jun. 1993.

[18] F. F. Dubrovka and B. S. Hardjosoekatmo, "Microwave septum orthomode transducer," German Patent DE4437594, May 1996.

[19] H. Wolf and M. Schneider, "Orthomode coupler for an antenna system," U.S. Patent 9,478,838, Oct. 2016.

[20] M. Hagensen, "Polarizer and a method of operating the polarizer," U.S. Patent 9,653,766, May 2017.

[21] J.-C. Angevain and N. J. G. Fonseca, "Directional coupler and a method of manufacturing thereof," U.S. Patent 10,957,965, Mar. 2021.

[22] N. J. G. Fonseca and J.-C Angevain, "Waveguide hybrid septum coupler," *IEEE Trans. Microw. Theory Techn.*, vol. 69, no. 6, pp. 3030–3036, Jun. 2021.

[23] I. Kim, J. M. Kovitz, and Y. Rahmat-Samii, "Sigmoid profiled septum: Evaluation of the parabolic reflector with the septum feed horn," in *Proc. IEEE Antennas Propag. Soc. Int. Symp.*, Orlando, USA, 2013, pp. 236–237.

[24] I. Kim, J. M. Kovitz, and Y. Rahmat-Samii, "Enhancing the power capabilities of the stepped septum using an optimized smooth Sigmoid profile," *IEEE Antennas Propag. Mag.*, vol. 56, no. 5, pp. 16–42, Oct. 2014.

[25] J.-C. Angevain and N. J. G. Fonseca, "Waveguide septum polarizer shaped with Legendre polynomials," in *Proc. 11th Eur. Conf. Antennas Propag.*, Paris, France, 2017, pp. 2286–2290.

[26] G. Addamo et al., "Additive manufacturing of Ka-band dual-polarization waveguide components," *IEEE Trans. Microw. Theory Techn.*, vol. 66, no. 8, pp. 3589–3596, Aug. 2018.

[27] K. Glatre, L. Hildebrand, E. Charbonneau, J. Perrin, and E. Amyotte, "Paving the way for higher-volume cost-effective space antennas: Designing for manufacturing, assembly, integration, and test," *IEEE Antennas Propag. Mag.*, vol. 61, no. 5, pp. 47–53, Oct. 2019.

[28] N. J. G. Fonseca, J.-C. Angevain, and C. Mangenot, "Toward the terabit/s satellite: Antenna design trade-offs and analyses," in *Proc. 33rd ESA Antenna Workshop*, Noordwijk, The Netherlands, 2011, pp. 1–8.

[29] B. Palacin et al., "Multibeam antennas for very high throughput satellites in Europe: Technologies and trends," in *Proc. 11th Eur. Conf. Antennas Propag.*, Paris, France, 2017, pp. 2413–2417.

[30] Y. Demers et al., "Ka-band user antennas for VHTS GEO applications," in *Proc. 11th Eur. Conf. Antennas Propag.*, Paris, France, 2017, pp. 2418–2422.
[31] J. L. Cano and A. Mediavilla, "On the accurate full characterization of septum polarizers through simple amplitude measurements in back-to-back configuration," *IEEE Trans. Microw. Theory Techn.*, vol. 69, no. 1, pp. 179–188, Jan. 2021.
[32] S. Rahiminejad et al., "Polymer gap adapter for contactless robust and fast measurements at 220–325 GHz," *J. Microelectromech. Syst.*, vol. 25, no. 1, pp. 160–169, Feb. 2016.
[33] O. Quevedo-Teruel, Q. Chen, F. Mesa, N. J. G. Fonseca, and G. Valerio, "On the benefits of glide symmetries for microwave devices," *IEEE J. Microwaves*, vol. 1, no. 1, pp. 457–469, Jan. 2021.
[34] T. A. Milligan, "Properties of antennas," in *Modern Antenna Des.*, 2nd ed. Hoboken, NJ, USA: Wiley, 2005, ch. 1, sec. 1– 11, pp. 18–27.
[35] M. Kilian, J. Kassner, P. Soboll, and M. Schneider, "Ku-band feed with integrated matrix power amplifier," in *Proc. 15th Eur. Conf. Antennas Propag.*, Dusseldorf, Germany, 2021, pp. 1–4.
[36] K. Kotzé and J. Gilmore, "SLM 3D-Printed horn antenna for satellite communications at X-band," in *Proc. IEEE-APS Topical Conf. Antennas Propag. Wireless Commun.*, Granada, Spain, 2019, pp. 148–153.
[37] N. J. G. Fonseca, Q. Liao, and O. Quevedo-Teruel, "Equivalent planar lens ray-tracing model to design modulated geodesic lenses using non-Euclidean transformation optics," *IEEE Trans. Antennas Propag.*, vol. 68, no. 5, pp. 3410–3422, May 2020.
[38] B. Deutschmann and A. F. Jacob, "Broadband septum polarizer with triangular common port," *IEEE Trans. Microw. Theory Techn.*, vol. 68, no. 2, pp. 693–700, Feb. 2020.
[39] A. A. Kirilenko et al., "Electromagnetic modeling and design of dual-band septum polarizers," *Appl. Comput. Electromagn. Soc. J.*, vol. 21, no. 2, pp. 155–163, Jul. 2006.

NELSON J. G. FONSECA (Senior Member, IEEE) received the M.Eng. degree in electrical engineering from Ecole Nationale Supérieure d'Electrotechnique, Electronique, Informatique, Hydraulique et Télécommunications (ENSEEIHT), Toulouse, France, in 2003, the M.Sc. degree in electrical engineering from the Ecole Polytechnique de Montreal, Montreal, QC, Canada, in 2003, and the Ph.D. degree in electrical engineering from the Institut National Polytechnique de Toulouse – Université de Toulouse, Toulouse, France, in 2010.

He is currently an Antenna Engineer for the Antenna and Sub-Millimetre Waves Section, European Space Agency, Noordwijk, The Netherlands. Since November 2020, he has been holding an Honorary Appointment as Professional Fellow with the University of Technology Sydney, Ultimo, NSW, Australia. He has authored or coauthored more than 260 papers in peer-reviewed journals and conferences, and has more than 50 patents issued or pending. His research interests include multiple beam antennas for space missions, beam-former theory and design, ground terminal antennas, transfer of technology from and to terrestrial systems, including 5G networks, and novel manufacturing techniques.

Dr. Fonseca is currently an Associate Editor for *IET Microwaves, Antennas and Propagation* (MAP) and IEEE TRANSACTIONS ON MICROWAVE THEORY AND TECHNIQUES (TMTT), and a Topic Editor of IEEE JOURNAL OF MICROWAVES (JMW). He is also the Chair of the IEEE MTT-S Technical Committee 29 (TC-29) on Microwave Aerospace Systems. He has been a Board Member of the European School of Antennas and Propagation (ESoA) since January 2019 and is also a coordinator of the ESA/ESoA course on Antennas for Space Applications, for which he was voted best lecturer by the participants of the 2020 edition. He is the elected EurAAP Regional Delegate representing Benelux for the term 2021–2023. He was the recipient of several prizes and awards, including the Best Young Engineer Paper Award at the 29th ESA Workshop on Antennas in 2007, an ESA Teamwork Excellence Award in 2020, multiple ESA Technical Improvement Awards, and the Best Applied Technology Antenna Paper Award at EuCAP 2022.

JEAN-CHRISTOPHE ANGEVAIN received the M.Eng. degree in telecommunications from the Ecole Nationale Supérieure des Télécommunications de Bretagne, Brest, France, and the M.Sc. degree in electronics and electrical engineering from University College London, London, U.K., in 1995.

In 1997, he joined Alcatel Espace (now Thalès Alénia Space), Toulouse, France, where he has held various positions of increasing responsibility with the Department of Spaceborne Antennas. As an Antenna Product Manager, he was in charge of the procurement of the Cryosat 1 and 2 antennas for the Siral instrument. At this position, he was also responsible for the design and the development of the telecommunication antennas of Arabsat 4AR and the radiometer altimeter antenna of Altika instrument for the French-Indian SARAL satellite. In 2007, he joined the European Space Agency, Noordwijk, The Netherlands, as an Antenna Engineer in the Antenna and Sub-millimetre Wave Section. He was in charge of several key R&D activities aiming at the development of a European large deployable reflector antenna. He provided support to several ESA telecommunication and Earth Observation projects, such as Alphasat, EDRS, Sentinel 3, Sentinel 6, and ROSE-L. In November 2020, he joined the Microwave Instruments Section at ESA, where he is responsible for the development of atmospheric radars and radiometric instruments.

Mr. Angevain co-organized and chaired the 37th ESA antenna Workshop on large deployable antennas in 2016. He was a member of the ECSS Group in charge of the update of standard for multipactor design and test. He was the corecipient of the Best Innovative Paper Award at the 32nd ESA antenna workshop in 2010 and of an ESA Teamwork Excellence Award 2020. He is also co-inventor of two patents. Since 2008, he has been a teacher with the European School of Antennas.